THE EFFECTS OF SPRAY PARTICLES
FROM THE PENETRATION
OF THIN TARGETS BY HYPERVELOCITY PARTICLES

(Final Report)

AD 602 706

TECHNICAL DOCUMENTARY REPORT NO. APL TDR 64-60

20 March 1964

Directorate of Materials and Processes
Aeronautical Systems Division
Air Force Systems Command
Wright-Patterson Air Force Base, Ohio
Project No. 3145, Task No. 314507
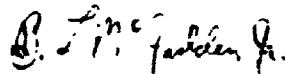
FOREWORD

ABSTRACT

When a thin bumper target is impacted by a hypervelocity particle, a spray of particles is produced. Data are presented on the penetration of these spray particles into a witness plate for various bumper and witness plate materials, spacings, and bumper thicknesses. The exploding-foil projection technique and associated diagnostics are also described.

This technical documentary report has been reviewed and is approved.

B. L. McFADDEN. Jr.
Acting Technical Manager
Dynamic Energy Conversion
Flight Vehicle Power Branch
Aerospace Power Division

TABLE OF CONTENTS

LIST OF ILLUSTRATIONS

CHAPTER 1

INTRODUCTION

Under Contract AF 33(657)-10615, Technical Operations Research investigated the effects of bumpers as a means of reducing penetration of high-velocity particles. Nearly ninety data points were collected from a series of high-velocity impacts in double-walled thin targets.

Target penetration for four different bumper-target spacings was investigated with various aluminum bumper-target combinations and bumper thicknesses. This procedure was repeated using constant spacing for aluminum and beryllium bumpers with columbium targets and for specially coated aluminum bumpers with aluminum targets. Data were also collected on the momentum transferred through thin targets of several thicknesses. All impacts were made with Mylar particles, 0.250 in. in diam and 0.010 in. thick. These particles had an original mass of 11 mg. They were projected by an exploding-foil gun fired by electrical energy supplied by a fast-discharge capacitor bank. Impact velocities ranged from 20,000 ft/sec to 30,000 ft/sec.

This program was carried out in the Tech/Ops-ASD Hypervelocity Facility over a 1 year period. Concurrently, work was done on Air Force Contract AF 33(616)-8423 to improve the efficiency and reliability of the particle projection method and the associated diagnostic techniques. Consequently, in the course of the year, the facility underwent several major modifications and work on the present contract was divided into two parts: (1) work performed before July, 1963, and (2) work performed after July, 1963. Continuity between the two sections was maintained, and the significance of the improvements is discussed where applicable to this contract in Chapters 2 and 3. Chapter 3 includes a discussion of the technique used to measure the momentum ratio across a thin target. In Chapter 4, the experimental data are presented.

CHAPTER 2

THE HYPERVELOCITY FACILITY

The Tech/Ops-ASD Hypervelocity Facility consists of an expendable, exploding-foil gun, an electrical energy-storage system, a vacuum system, and associated diagnostic equipment — a Beckman & Whitley streak camera, a backlighting source, a Beckman & Whitley Dynafax camera, and crater profile tracing equipment. A block diagram of the overall system is shown in Figure 1.
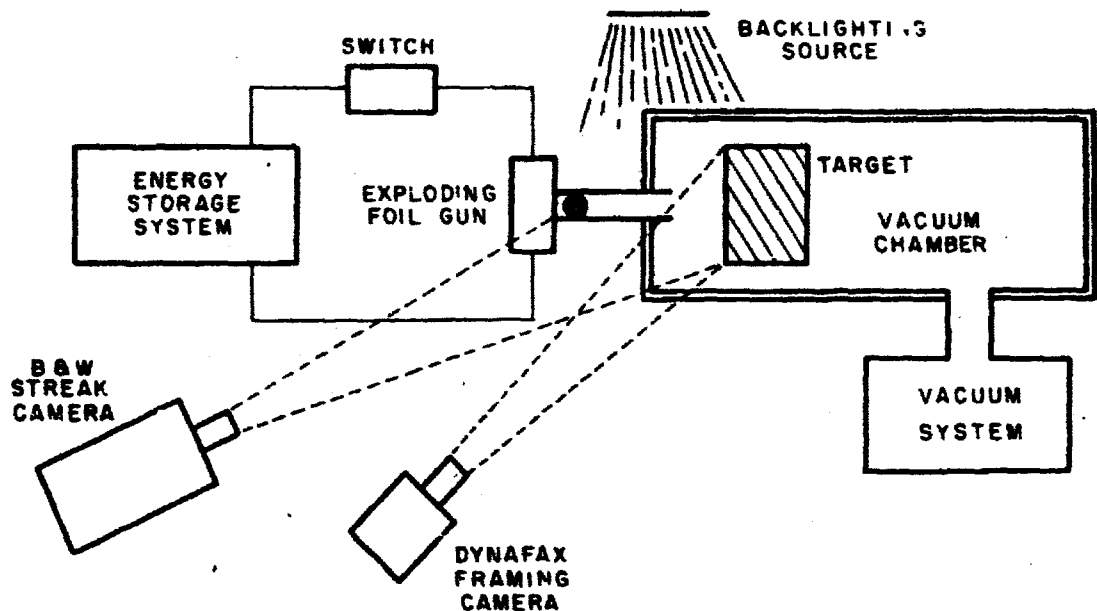
Figure 1. Block Diagram of Hypervelocity System

In operation, a foil is placed in the breech area of the gun, and the gun is powered by an electrical discharge from the energy storage system. The hot gas generated by the explosion punches a particle from the foil and expels it from the gun. The particle then bombards the target. The diagnostic equipment records phenomena during impact, such as the light emitted and particle velocity. Other effects of target impact, such as crater volume, are measured later with the profile tracing equipment. The important features of the present hypervelocity system are depicted schematically in the exploded diagram in Figure 2.

Figure 3 shows the gun used to fire the shots for this contract. This gun fires an 11 mg disc, 0.250 in. in diam and 0.010 in. thick, 20,000 to 30,000 ft/sec. All the impacts performed on this contract were done with this gun, but during the contract period the discharge system was extensively modified. The first half of the work was done with one of two 8 μF capacitor banks storing 10,000 J at 50 kV (Figure 4). The discharge frequency of the system was 60 kc-65 kc: the gun used was very well matched to this circuit. The laboratory layout for this arrangement is shown in Figure 5.

FOLDED AL FOIL
1 MIL BY 1 CM

MYLAR FILM, APPROX
10 MIL BY 1 CM BY 1 CM

LUCITE
BACKSTOP

1/4"

LUCITE
BARREL

FIBERGLAS
OR MYLAR
INSULATION
10 TO 50 MIL

TRIGGER
GAP

4
μ f

APPROX
100 KV
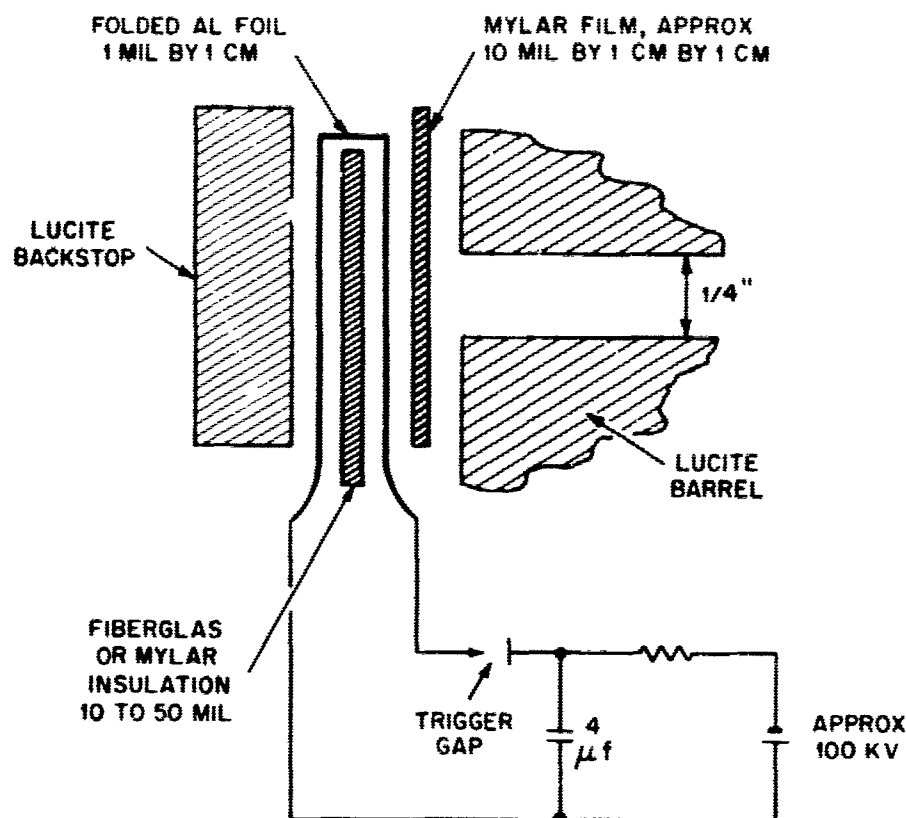
Figure 2.   Exploded Diagram of Present Hypervelocity System

In July, 1963, the discharge system and velocity measuring technique were modified and improved. (See Chapter 3.) The gun room used to protect personnel and equipment was rotated 90° and was moved closer to the capacitor banks (Figure 6) where both banks were connected in series through a low-inductance, parallel-plate, transmission line (Figure 7). This discharge system stored 20,000 J at 100 kV, and its discharge frequency was 117 kc-120 kc. Because of the change in discharge characteristics of the system, it was necessary to change some parameters in the gun design to take better advantage of the higher total energy and higher power input. However, for the sake of continuity, the same gun design was used for both series of impacts, although the performance of the gun was slightly better in the new system.

The average velocity for more than 75 single impact shots was slightly better than 20,000 ft/sec with the single bank arrangement; in the two-bank arrangement, the average velocity was about 25,000 ft/sec. Since some improvement was shown, a series of shots was repeated in the new system for one set of target conditions for comparison purposes as plotted in Figure 16c (see p. 21). The physical arrangement of the gun and target is such that the path of the projectile is evacuated to 10 μ–30 μ for most shots fired. The exceptions were the five beryllium shots in which pressures were near 1000 μ because of filters in the vacuum system that were necessary to prevent contamination.
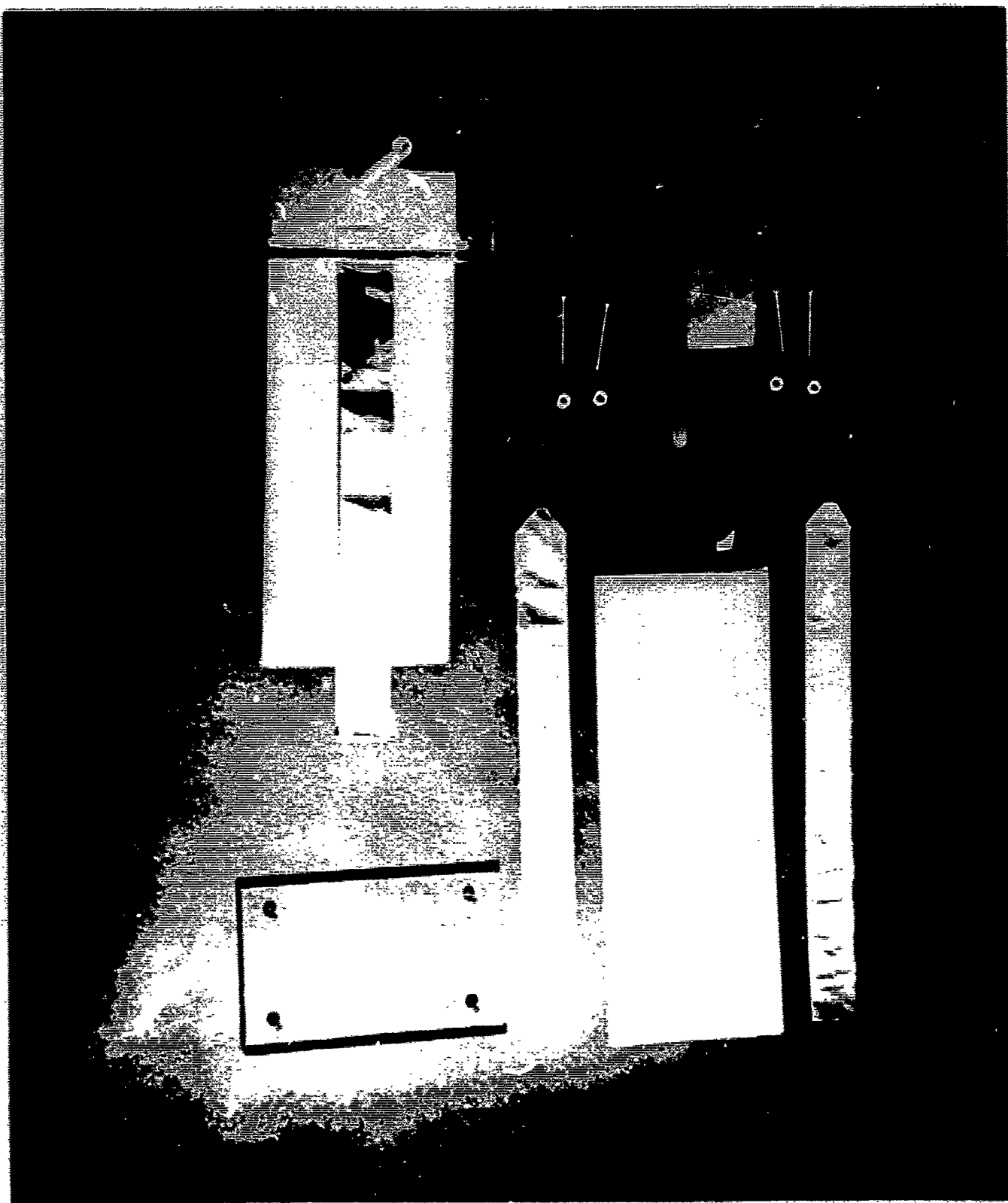
Figure 3. Picture of Gun Used for Work on This Contract
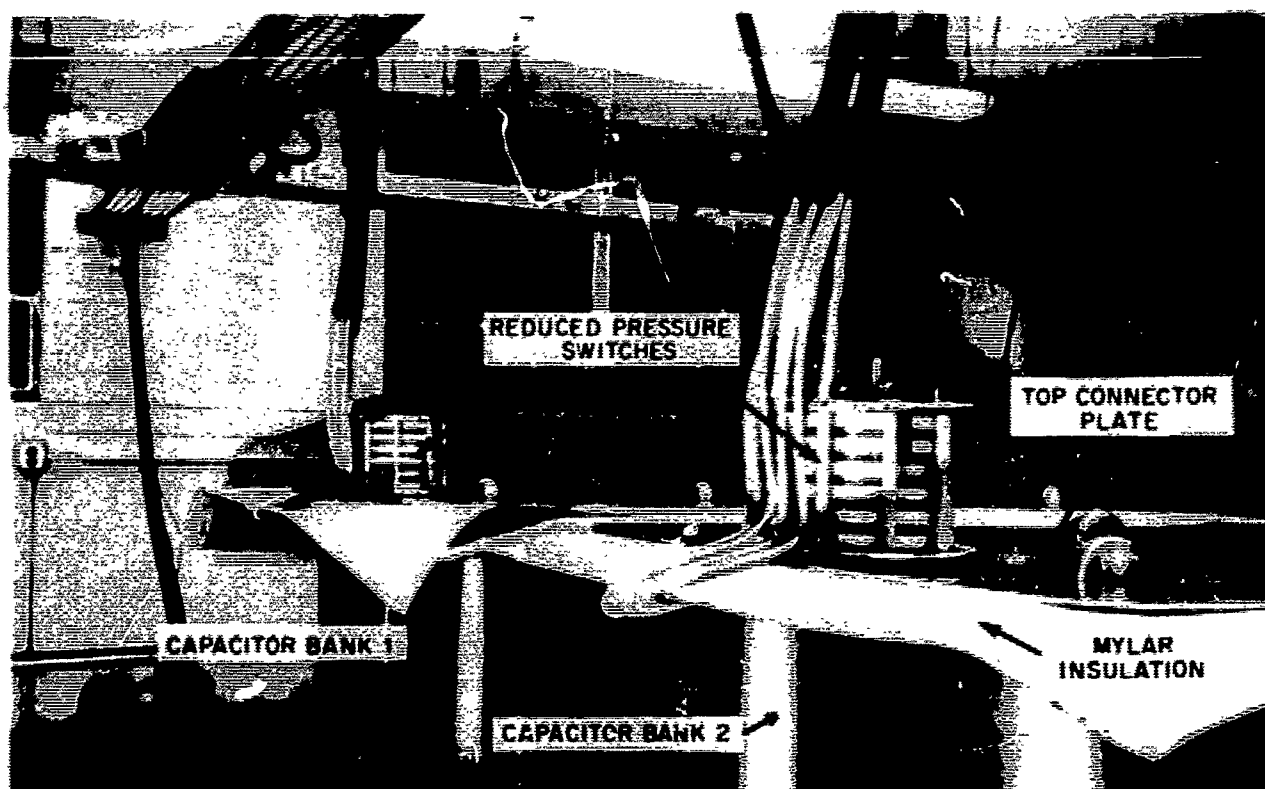
Figure 4. Two $8\,\mu F$ Capacitor Banks
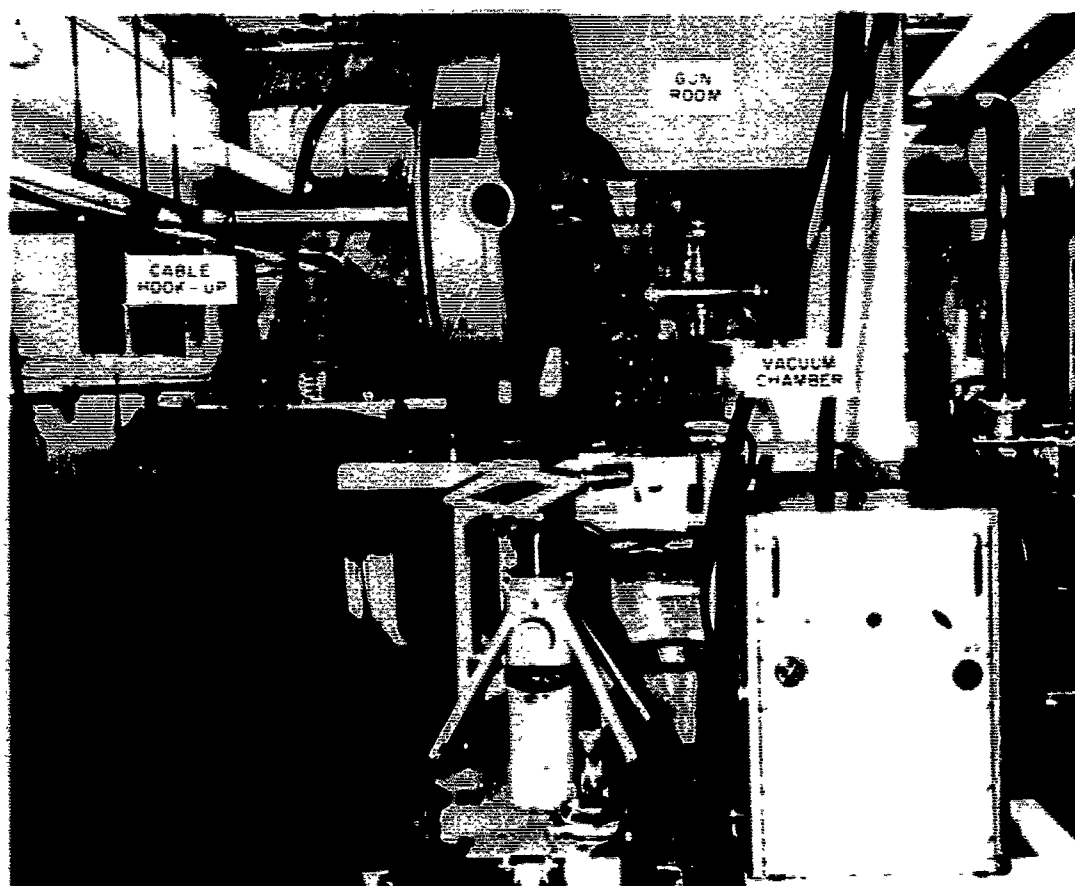
Figure 5. Laboratory Layout Prior to July 1963
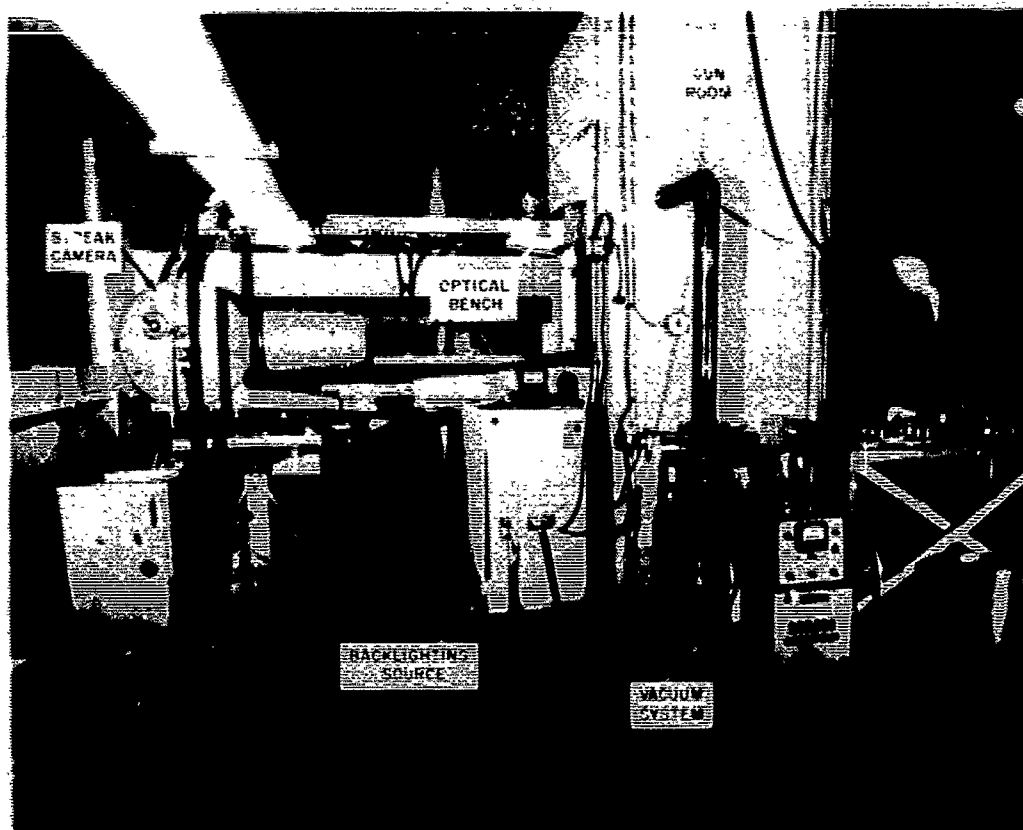
Figure 6. Present Laboratory Layout
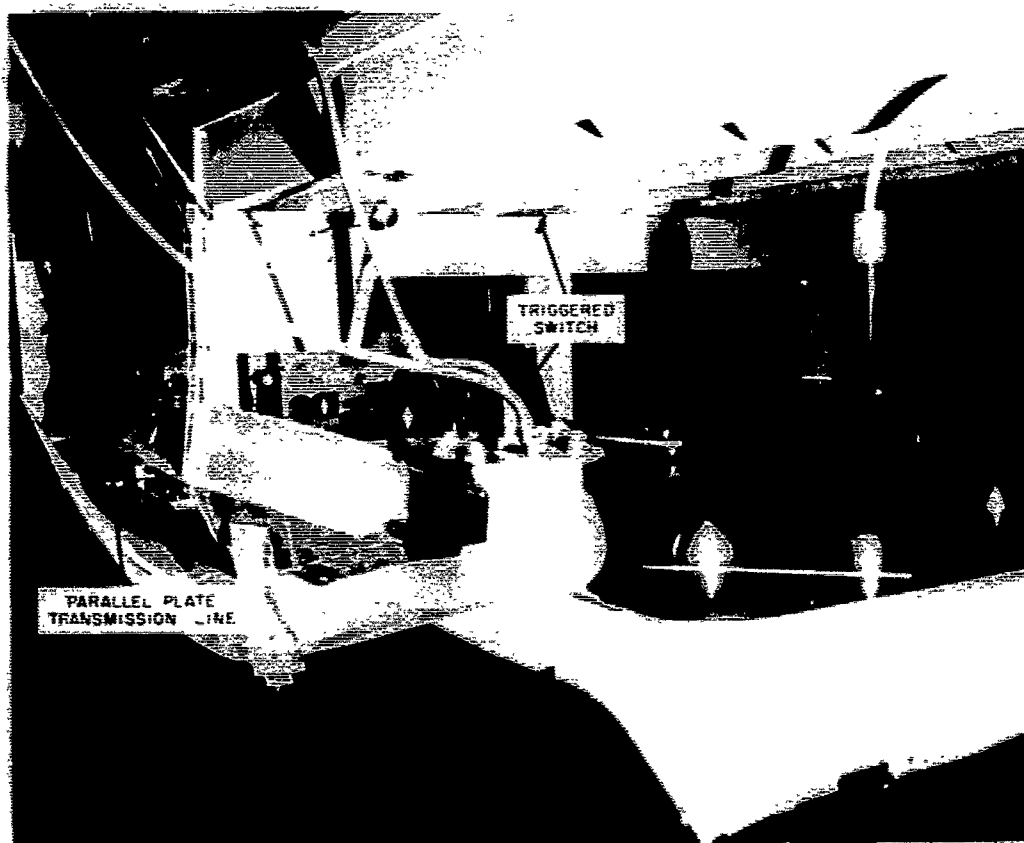
Figure 7. Parallel-Plate, Transmission Line Series Arrangement
of Two 8 μF Capacitor Banks

CHAPTER 3

DIAGNOSTIC EQUIPMENT

VELOCITY MEASUREMENTS

By July, 1963, all the impacts required by the contract were completed except the beryllium bumpers and the special targets to be furnished by ASD. This work was finished in December, 1963. In the intervening time, improvements in diagnostic techniques brought to light discrepancies in our velocity measurements.

The first step in the evolution of a reliable velocity-measurement technique that could be used to measure the velocity of a small particle propelled by hot and very dense radiating plasmas was described in ASD-TDR-62-762 (August, 1962).* This description was written under Contract No. AF 33(616)-8423 and applies to all work done prior to July, 1963. The primary assumption underlying that work was that a high particle velocity was the necessary consequence of high propellant-plasma velocity. To implement this idea, exploding-foil guns were developed (see Figure 1) that accelerated aluminum plasmas to velocities in excess of 250,000 ft/sec.

When these same guns were used to propel a light disc-shaped particle, the velocity measured from a uniform, self-luminous plasma front was one fifth that of the free expansion. To measure the velocities, the exploding-foil gun was arranged so that the center line of the gun barrel, breech, and target was focused on the slit of the streak camera by the objective lens (Figure 8). Thus, we could observe the initial, contained-foil explosion, the rupture of the particle disc, and the expansion of the hot propellant gas.

When used in this manner, the streak camera did not see the accelerated particle in the gun, but rather recorded the position of the propellant plasma as a continuous function of time. From this observation, the velocity of plasma propagation was determined on the assumption that the propellant plasma was pushing the particle. Thus, the measurement of plasma velocity was assumed to be a measure of particle velocity. This method of deducing particle velocity was used extensively in our experiments. Since the equilibrium position for a flat disc in a uniform gas flow is such as to present maximum area, the marked difference in the plasma velocity for guns with, and without, a particle was assumed to be due to its confinement by the small disc; if so, the particle moved at the measured expansion velocity. A perfect gas seal was most improbable at the very high pressures involved, and there was some evidence of leakage. In front of the assumed particle position, some very low density gas was seen moving at about twice the velocity of the very dense plasma thought to be propelling the particle. Whenever the particle was shattered in the initial expansion, the front of the plasma expansion became very diffuse, and the velocity was 30% to 40% higher than any recorded for a single particle impact. From this evidence, it seemed that our assumption was sound.

In the summer of 1963, however, a photographic technique was developed that could penetrate the very bright and nearly opaque plasma around the particle. It was found that the particle lagged behind the plasma so that particle velocities were 40% to 50% lower than that of the dense plasma front. This new discriminating photographic technique was described in the Eighth Quarterly Progress Report.†

---

*V. E. Scherrer, "Effects of Hypervelocity Impacts on Materials," Technical Documentary Report No. ASD-TDR-62-762 (August, 1962).

†V. E. Scherrer, H. Stevens, and R. W. O'Neil, "Effects of Hypervelocity Impacts on Materials," Technical Operations, Incorporated, Report TO-B 63-89 (4 October 1963).
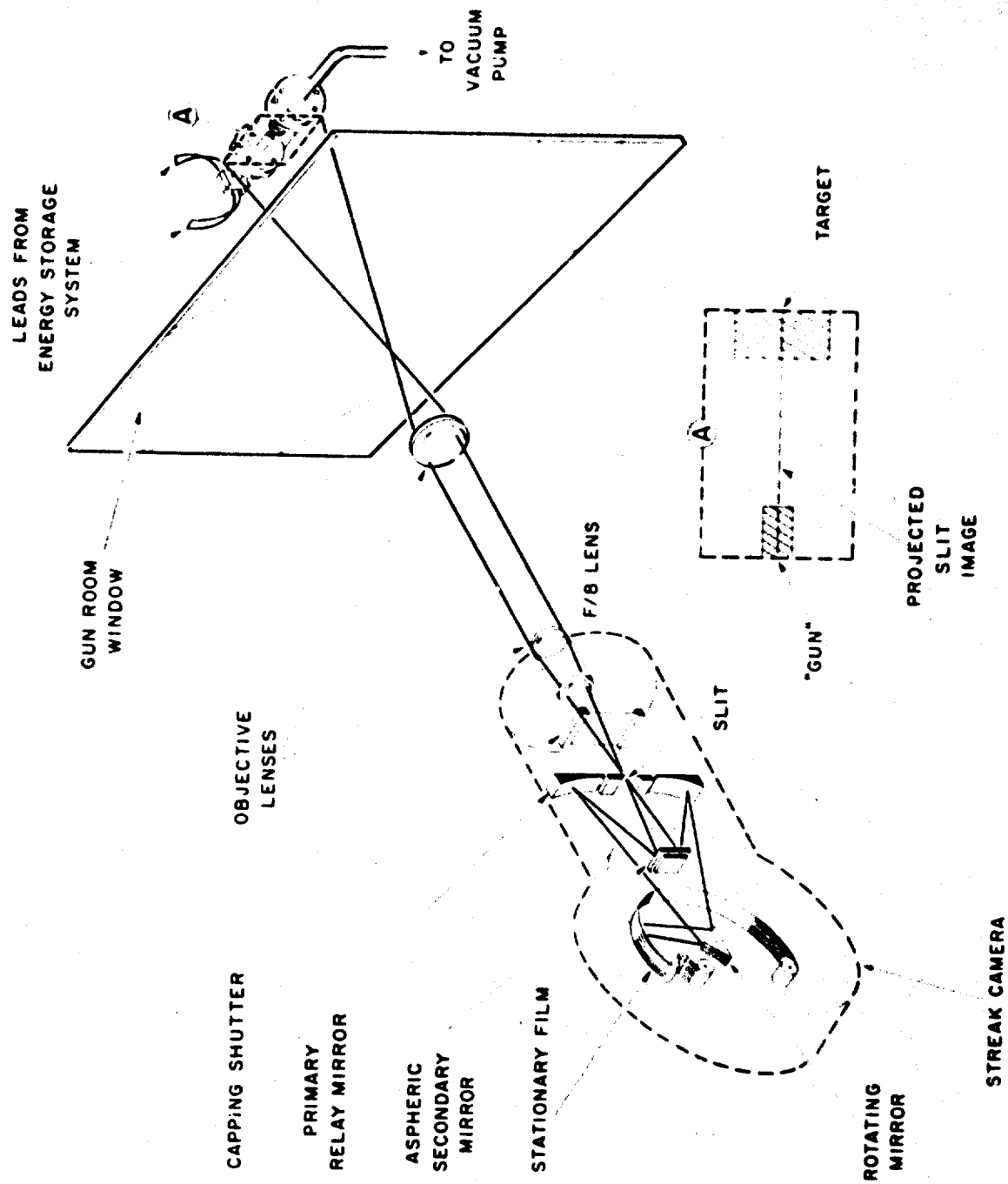
Figure 8. Method of Measuring Particle Velocity from Plasma Expansion

LEADS FROM
ENERGY STORAGE
SYSTEM

TO
VACUUM
PUMP

A

GUN ROOM
WINDOW

OBJECTIVE
LENSES

CAPPING SHUTTER

PRIMARY
RELAY MIRROR

ASPHERIC
SECONDARY
MIRROR

STATIONARY FILM

ROTATING
MIRROR

F/8 LENS

SLIT

"GUN"

TARGET

A

PROJECTED
SLIT
IMAGE

STREAK CAMERA

8

OPTICAL SYSTEM

The basic optical system consists of a high-intensity point light source, an Aero Ektar f/2.5 7-in. achromatic collimating lens, and f/5.6 15-in. achromatic objective lens, a telecentric stop, a filter holder, and a film holder. The light source is imaged at the telecentric stop, which allows all the collimated light to reach the slit plane. Of the light originating at the object plane, however, only that parallel to the optical axis passes through the telecentric stop, and most of the light from the object plane is eliminated. The backlight duration and effective exposure time are adjusted such that the backlighting exceeds the particle transit time across the field by about a factor of 2.

Streak Pictures

Since the use of the streak camera to take simultaneous streak and framing pictures involves a complicated geometry, we will use Figures 9 and 10 to explain its operation. As indicated in the basic optical system shown in Figure 9, the object plane is imaged on the slit of the streak camera, which has its regular objective lens replaced by the second lens. In operation, an image of the slit is focused on the stationary film of the camera by its internal-relay optical system. The light beam is reflected onto the film by a prism-shaped mirror that rotates at high speed. The rotation of the mirror sweeps the slit image along the stationary film at a speed determined by the rate of mirror rotation and the length of the rotated beam. When the turbine rotates at a speed of 2500 rps, the image sweeps at a rate of 0.9 cm/μsec on the film. Minimum slit width is approximately 5×10^{-3} cm and the internal relay optics have a magnification of 0.5. The time resolution of the camera is the time required to sweep one slit width on the film, or 3×10^{-9} sec. Any displacement that occurs along the front slit of the streak camera is swept as a continuous function of time along the film in the camera. The camera, therefore, records displacement in one dimension as a continuous function of time.
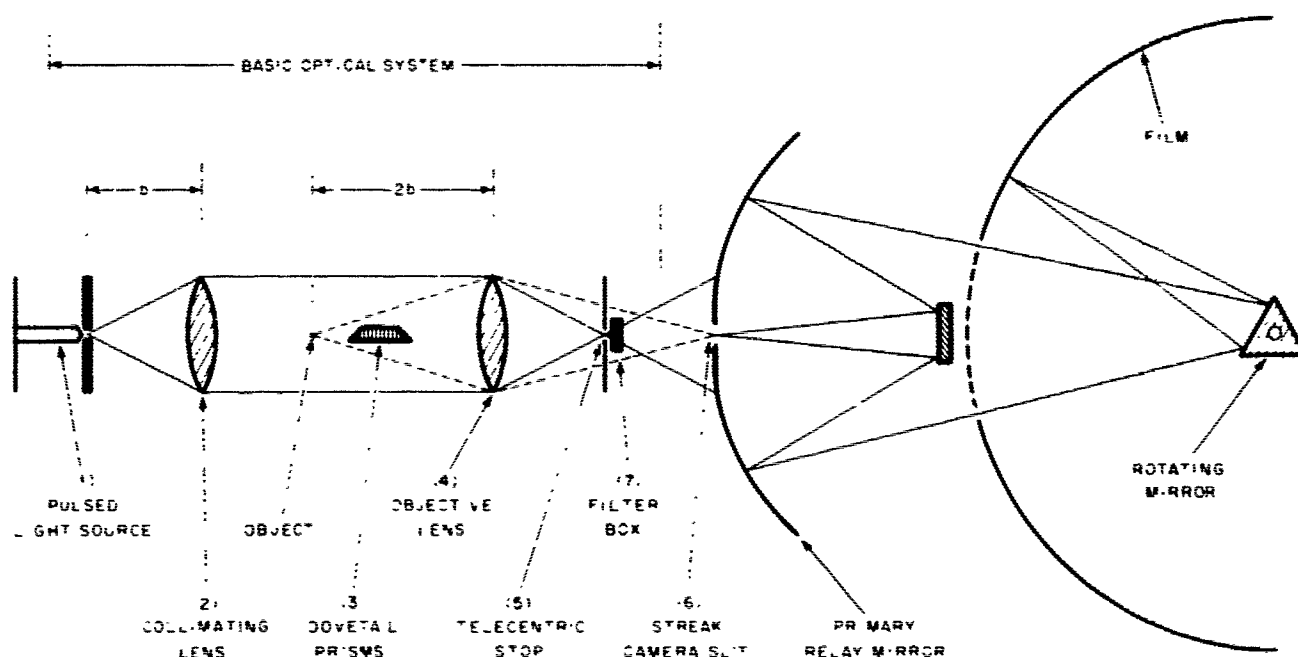
Figure 9. Schematic Diagram of Basic Optical System Modified for Use with Streak Camera

Framing Pictures

To take simultaneous streak and framing pictures that are also backlighted, several changes were made in the arrangement described above (see Figure 10). Photographing with a streak camera requires the insertion of dovetail prisms into the optical system. When set at the proper angle, these prisms rotate part of the image on the camera slit plane. This rotation of the object relative to the slit at the camera slit plane can be thought of as rotating a section of the projected slit image at the object plane, as indicated by inset A in Figure 10. Figure 11 illustrates how the picture is taken and shows the projected slit image (dotted line) at the object plane; the gun, particle trajectory, and target are also shown at this plane.
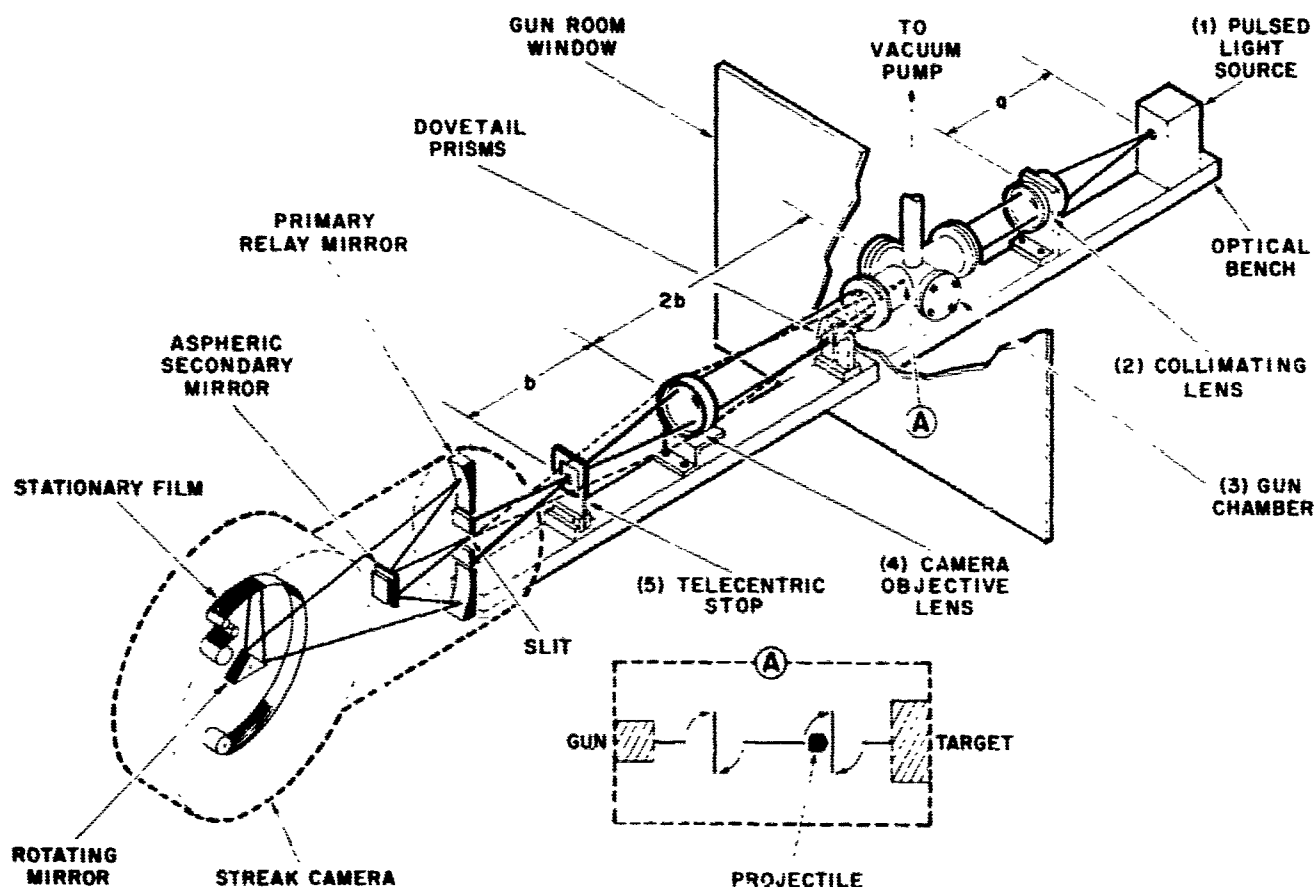
Figure 10. Method of Measuring Particle Velocity

When the particle moves along the trajectory from A to B (see Figure 11), a shadow streak is traced on the film A' to B'. When the particle travels from B to C, it crosses the rotated section of slit and traces its image on the film B' to C'. A similar image is traced on the film between D' and E' when the particle travels between D and E. Streak shadows are recorded on the film C' to D' and E' to F' as the particle follows the trajectory from C to D and E to F. If the impact results in the splash of dense material from the target, a shadow will be noticeable on the film F' to G'. Using this method, one can insert additional dovetail prisms and obtain one frame for each one inserted.

10

The number of prisms that can be thus inserted is limited by the physical size of the particle to be observed and by the magnification of the optical system. For small particles or for low magnification, smaller dovetail prisms can be used and six or twelve frames can easily be obtained. If additional pictures are required, some sacrifice will have to be made in the length of streak record. For our present program, two frames with a good streak record are adequate.

Another slight modification to the conventional photographic arrangement is required to take backlighted streak pictures with the Beckman & Whitley Model 339B Streak Camera. In norma' use, the internal relay optics of the camera are arranged such that light from the primary relay mirror to the rotating mirror passes to one side of the film holder. With the optical arrangement shown in Figure 10, this is possible only if one quarter of the area of the primary relay mirror is used and the camera is angled for alignment. This changes slightly the effective f-number of the system.
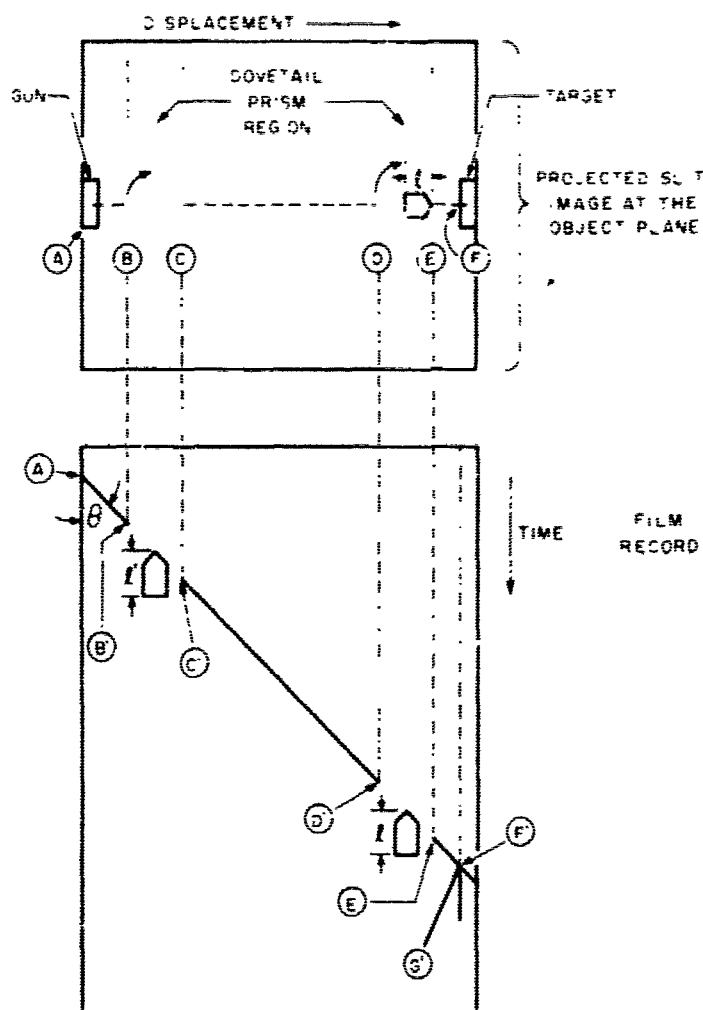
Figure 11.   Method of Taking Velocity-Synchronized Streak Pictures

With this modification, the effective exposure time for taking pictures is the time the image takes to move one slit width on the film. For a slit width of 5×10^{-3} cm, this is 3×10^{-9} sec. However, if the particle image on the film is traveling at the same speed as the camera writing speed, they are velocity-synchronized[*] with no relative motion. Therefore, the picture quality is improved even more than the exposure time would indicate. The image is velocity-synchronized (see Figure 11) when the angle Θ is equal to 45°. If the image is not velocity-synchronized, the image size will be expanded $(\Theta < 45°)$ or contracted $(\Theta > 45°)$ along the time axis. That is, dimension ℓ' is equal to ℓ' if $\Theta = 45°$, and ℓ is smaller than ℓ' if $\Theta < 45°$. In Figure 12, we show four streak-framed photographs of particles in flight.

Each individual shot fired after July 1963 has a velocity recorded in this manner: the shots fired before this time do not, and there is some uncertainty as to the velocity of any one shot. However, the gun used for this contract was fired in the unmodified discharge system over 75 times with an accurate record of each individual velocity. For this gun, the average velocity was 21,000 ft/sec with a deviation of less than 1500 ft/sec for single particle impacts.

―――――――――
[*] The idea of "velocity synchronization" was suggested by T. Holland, Beckman & Whitley, Inc.

11

a. Taken at 23,900 ft/sec
   Particle 1/8-in. diam 0.010-in. thick Mylar

b. Taken at 26,500 ft/sec
   Particle 1/4-in. diam 0.010-in. thick Mylar

c. Taken at 20,000 ft/sec
   Particle 3/16-in. diam 0.010-in. thick Mylar

d. Taken at 23,000 ft/sec
   Particle 1/4-in. diam 0.010-in. thick Mylar

Figure 12. Streak Framing Picture of Particles in Flight

MOMENTUM RATIO ACROSS A THIN TARGET

To measure the momentum ratio, the momentum of a secondary target is measured and is compared with the incident particle momentum. This method features a low density target designed to trap the momentum of a given mass and velocity. This target design (see Figure 13) uses a very light canister filled with a predetermined number of thin aluminum sheets (0.005 in. → 0.010 in.) and relatively thick Styrofoam absorbers. The weight of these targets can be varied from 1 g to 20 g as the mass and velocity range are changed. The open end of the target is covered with a thin foil Mylar laminate (0.003 in. total thickness) that allows the particles to enter the target easily but is strong enough to eliminate target-mass losses during impact and to trap any recoil momentum (except for that lost out the small hole through which the particles enter). At each interface, the particle loses some mass as vapor and small fragments, and these are captured by the absorbing material.
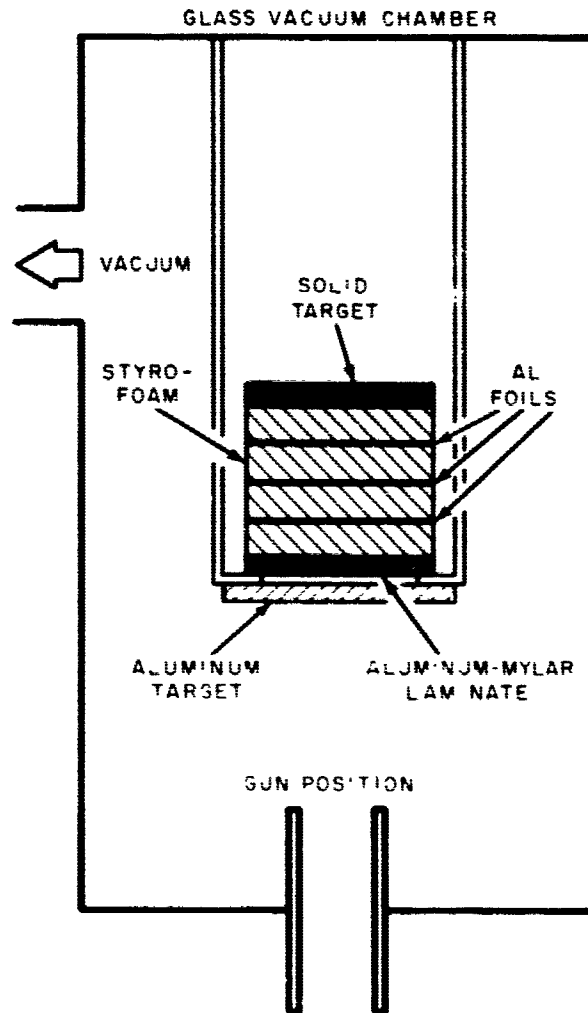
Figure 13. Configuration for Measurement of the Momentum Ratio Across a Thin Target

By this technique, the normal momentum is conserved without introducing additional accelerations. Measurements are taken in the vertical direction in less than 2 msec over distances of about 2 cm. The target velocities are measured with a Beckman & Whitley Dynafax Framing Camera that can take 224 well-resolved data frames in times as short as 9 msec (see Figure 14). For analysis, each frame is magnified twenty times, and 98% accuracy is possible in target velocity determination.

The incident particle momentum has been measured by this technique in over 250 independent shots. Particle velocity is measured with the streak camera and at least 90% of the incident particle momentum is transferred to this small canister target. In Chapter 4, Figure 19, the ratio of target momentum to particle momentum is plotted as a function of bumper thickness.

DYNAFAX FRAMING CAMERA

The Beckman & Whitley Dynafax Camera in Figure 14 is used primarily for observing slow moving events associated with target impacts. The camera has a maximum framing rate of 25,000 fps.

CRATER MEASURING DEVICE

Figure 15 shows the device used to measure the depth and the diameter of the target craters resulting from hypervelocity impact. The device consists of a precision micrometer crossfeed table and long-reach dial indicator that permit depth measurement to within 0.001 in. and diameter measurements, in two directions. to within 0.0001 in.
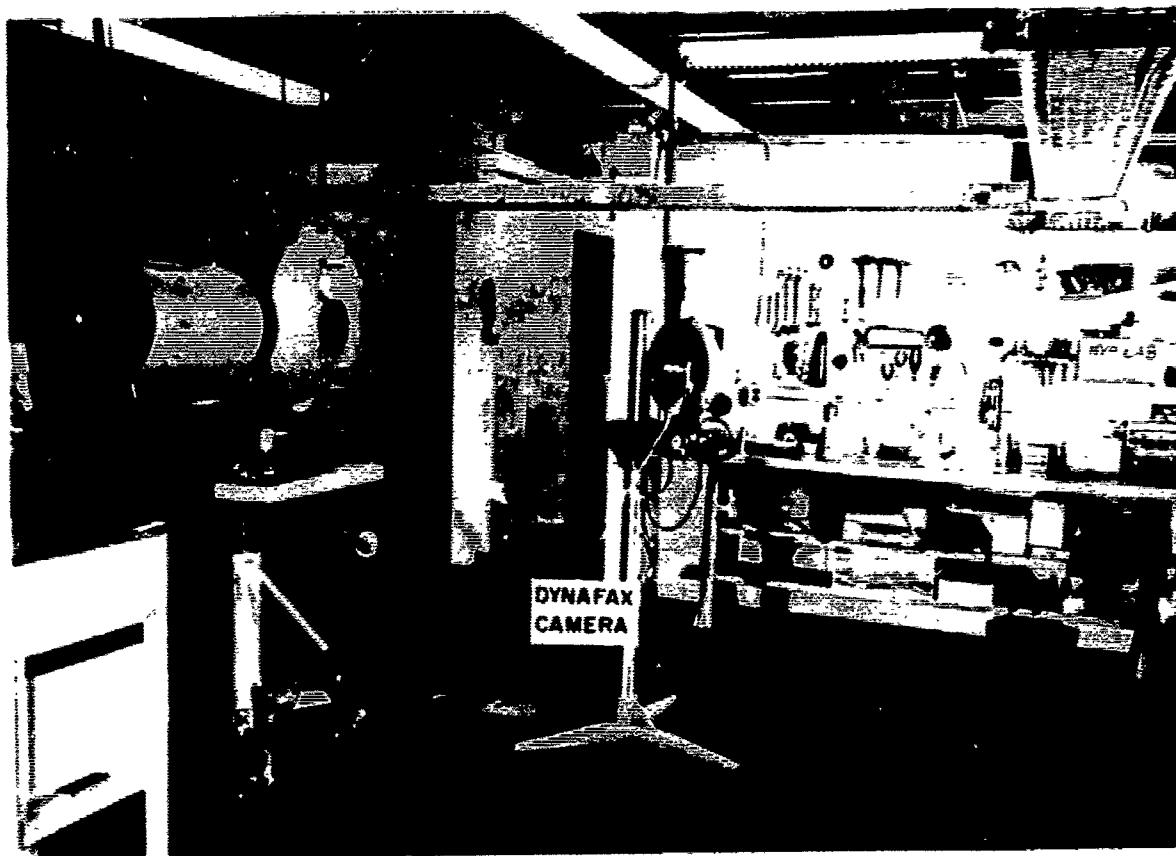
Figure 14. Beckman & Whitley Dynafax Framing Camera

14

Figure 15. Crater Profile Tracing Equipment

CHAPTER 4

EXPERIMENTAL DATA

The purpose of this program was to investigate the penetration of a witness target by spray particles from a thin bumper in front of the target after this bumper has been penetrated by a small, low-density, hypervelocity particle. To satisfy this requirement, nearly ninety data points were collected. About half of the impacts were performed in each firing period. In the first set, the velocity range is estimated to be 21,000 ft/sec ± 1500 ft/sec, although no reliable data 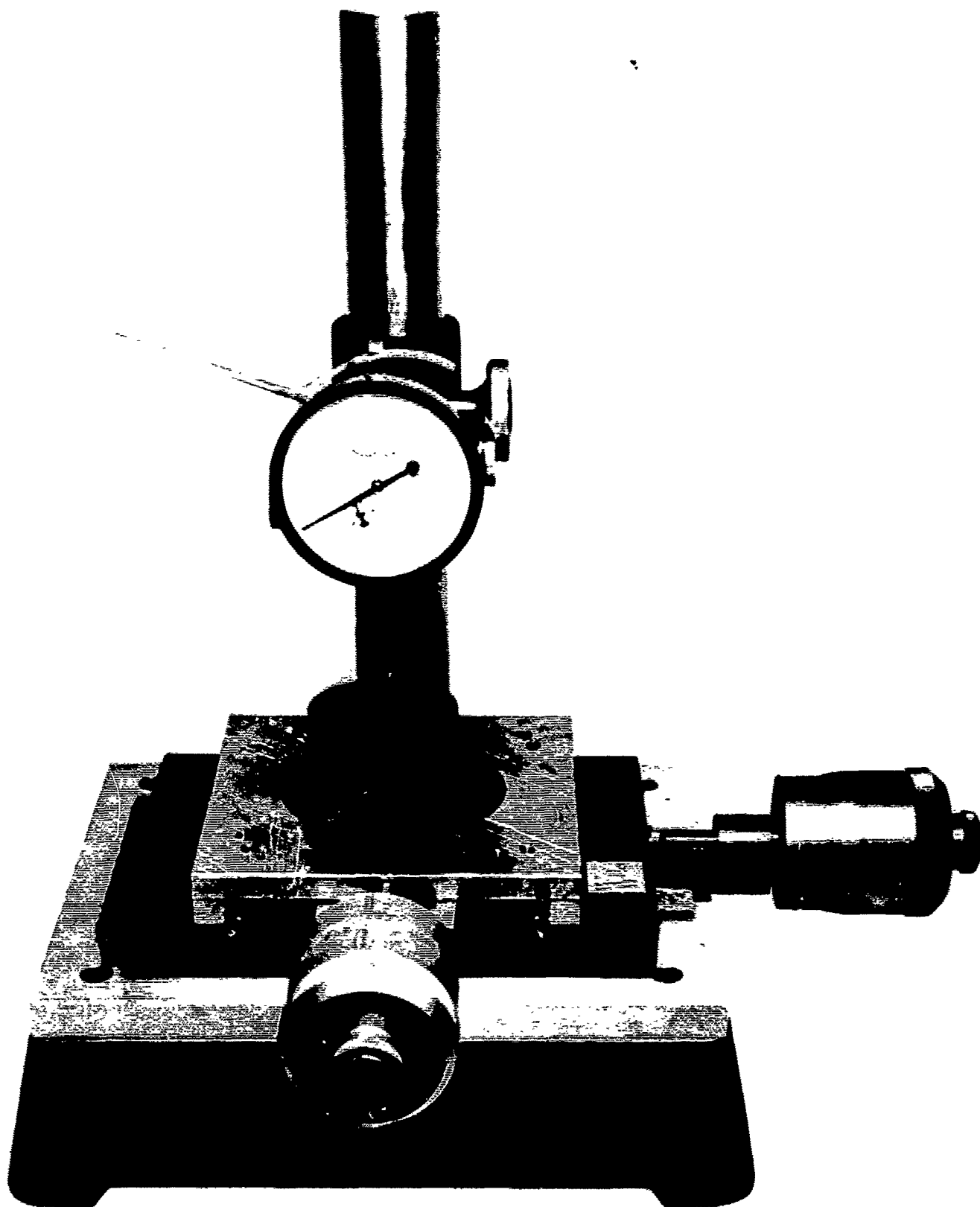exist on any particular shot. This estimate is based on the average velocity of over seventy-five single particle impacts fired under conditions identical to the shots fired for this contract, except that for each individual shot an accurate velocity was recorded. In the second set, the velocity range was 22,500 ft/sec to 28,500 ft/sec with an average near 25,000 ft/sec.

All of the experimental data are tabulated in Tables 1-3, in chronological order. Tables 1 and 2 give the data taken during the first half of the contract period. Table 3 gives data for the second half of the contract.

TABLE 1
MYLAR PARTICLE IMPACTS IN BUMPER-TARGET SERIES

Shot No	*	Bumper Thickness (in.)	Spacing (in.)	Max Depth of Penetration (in.)	Shot No	*	Bumper Thickness (in.)	Spacing (in.)	Max Depth of Penetration (in.)
				2024 Aluminum - Aluminum					
3047		0.025	1/4	0.027	3066		0.102		
3048		0.050			3067		0.046		
3049		0.046							
3050		0.102			3069		0.025		
3051		0.125					0.025		0.045
3052		0.161			3071				
3053		0.005							
3054		0.010	1/4				0.025		
3055		0.005	1/2						
3056		0.016							
3057		0.025							
3058		0.036					0.161		
3059		0.046					0.125		
3060		0.102							
3061		0.125			3081				
3063		0.161							
3065		0.125					0.025		
				Aluminum - Columbium					
3064		0.161	1/2		3090				
3065		0.125			3091				
3066		0.102							
3067		0.046			3452				
3068		0.050							
3069		0.025			3434		0.025	1/2	
					3436				

*Velocity 21,000 ft/sec ± 1500 ft/sec

Best Available Copy

16

TABLE 2

MOMENTUM RATIO DATA

Shot No.	Bumper Thickness (in.)	Transferred Momentum (g-cm/sec)	Incident Momentum (g-cm/sec)	Moment Ratio
3094	0.010	10,000	9,100	1.1
3095	0.025	9,450	9,450	1.0
3096	0.050	7,400	10,000	0.740
3097	0.005	7,200	8,500	0.845
3102	0.080	6,100	8,900	0.690
3125	0.161	0	9,100	0
3126	0.005	11,800	9,500	1.24
3129	0.102	2,500	8,900	0.280
3130	0.125	4,650	9,300	0.500

TABLE 3

MYLAR PARTICLE IMPACTS IN BUMPER-TARGET SERIES
(1 in. Spacing)

Shot No.	Velocity (ft/sec x 10^4)	Thickness of Bumper (in.)	Max. Depth Penetration (in.)	Shot No	Velocity (ft/sec x 10^4)	Thickness of Bumper (in.)	Max. Depth Penetration (in.)
			2024 Aluminum Bumpers and Targets				
3911	2.36	0.025	0.026	3918	2.50	0.102	0.018
3912	2.02	0.025	0.027	3919	2.60	0.125	0.007
3913	2.6~	0.025	0.023	3920	2.50	0.050	0.011
3915	2.45	0.025	0.019	3921	2.47	0.161	
3916	2.50	0.050	0.013				
			Aluminum Bumpers with Special Coatings				
3949	2.40	0.013	0.036	3964	2.60	0.032	0.018
3950	2.~~	0.013	0.048	3965	2.32	0.032	0.017
3951	2.50	0.032	0.067	3966	2.30	0.013	0.016
3952	2.30	0.030	0.016	3967	2.42	0.032	0.014
3953	2.25	0.065	0.021	3968	2.55	0.013	0.050
3954	2.30	0.040	0.017	3969		0.050	0.021
3955	2.30	0.090	0.015	3971	2.60	0.090	0.007
3956	2.30	0.125		3972	2.50	0.032	0.018
3957	2.55	0.176		3973	2.75	0.050	0.017
3958	2.43	0.176	0.004	3974	2.62	0.090	0.016
3959	2.30	0.125	0.005	3975	2.50	0.125	
3960	2.~~	0.090	0.011	3983	2.40	0.065	0.029
3962	2.~~	0.065	0.012	3984	2.~2	0.065	0.011
3963		0.050	0.020	3985	2.45	0.032	0.013
			Beryllium Bumpers and Columbium Targets				
3989	2.4~	0.043	shattered	3992	2.30	0.250	cracked and spalled
3990	2.66	0.06~	shattered				
3991	2.40	0.130	cracked and spalled	3993	2.30	0.375	very light surface damage. particle breakup probable

17

The experimental data consist of plots of the maximum penetration depth in the witness target as a function of the various parameters. This depth is the maximum penetration beneath the undamaged surface measured with a probe 0.020 in. in diameter.

The actual firing was divided into six groups:

1. For a constant bumper-target spacing, eight different bumper thicknesses (0.005 in., 0.010 in., 0.025 in., 0.050 in., 0.080 in., 0.102 in., 0.125 in., and 0.161 in.) were impacted.

2. Series 1 was repeated for a total of four bumper-target spacings (1/4 in., 1/2 in., 1 in., and 2 in.) In series 1 and 2 all targets and bumpers were 2024 aluminum, except that the 0.005 in. and 0.010 in. thick bumpers were 1100 aluminum. (In these thicknesses 2024 aluminum is not commercially available, but, in such thin targets, material properties should not be too significant.) Target thickness was held constant at 0.161 in. Data from these two series were plotted in Figure 16. In Figure 17, data taken before and after the system modification were plotted together for comparison purposes.

3. A series of shots were fired in which the witness target was 0.125 in. columbium. The aluminum bumpers, identical with those in the first two series, were spaced 1/2 in. apart. These data are plotted in Figure 18.

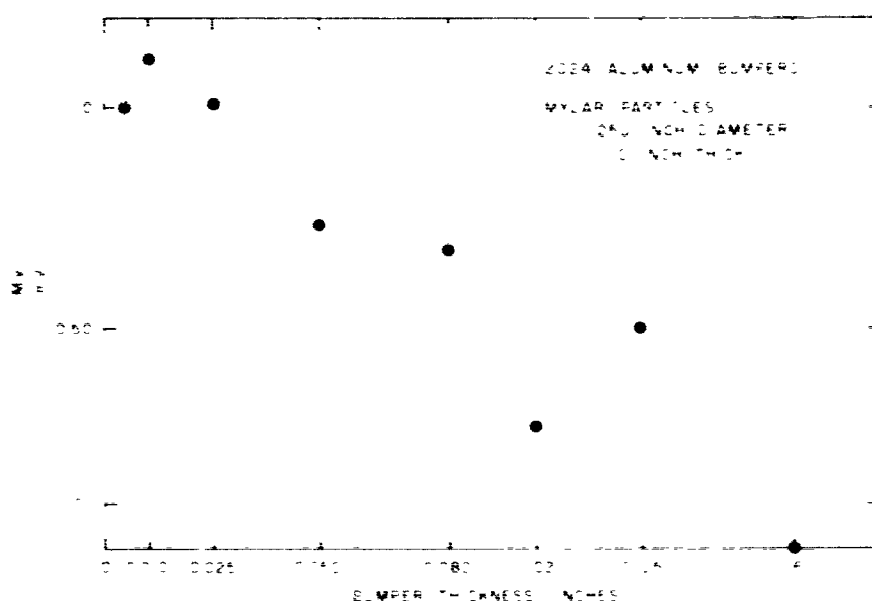Figure 16. Plot of Maximum Depth of Penetration in Witness Target as a Function of Bumper Thickness for Four Spacings. Bumpers and Targets Are 2024 Aluminum; Mylar Particles 0.25 in. Diam, 0.010 in. Thick

Figure 17. Comparison of Early Data with That Obtained Using
the Improved Velocity Measuring Equipment

Figure 18. Plot of Maximum Depth of Penetration as a Function
of Bumper Thickness for Special Targets and Bumpers

4. Five beryllium bumper-columbium target combinations spaced 1 in. apart were impacted. Bumper thicknesses were 0.043 in., 0.060 in., 0.130 in., 0.250 in., and 0.375 in. The first two bumpers were shattered into several pieces. The 0.130 in. and 0.250 in. bumpers cracked and spalled, and on the last target there was only a little light surface damage. The velocity record revealed the particle was shattered in the acceleration phase. Because of the hazards that accompany the handling of beryllium, no further analysis was attempted. The bumpers and targets from this series were placed in polyethylene bags and have been returned to ASD.

5. Twenty-eight specially coated aluminum bumpers supplied by ASD were successfully impacted. Bumper-target spacing was 1 in. These targets were returned, together with nine 2024 aluminum bumper target combinations included for comparison purposes. The impact velocity for each is included in the data in Table 2. A plot of penetration depth vs bumper thickness is presented in Figure 18.

6. Eight data points were collected on the momentum transferred across a thin target by measuring the momentum transferred to a special target that trapped the pieces of the target removed by the incident particle. This was compared with the incident particle momentum for eight different bumper thicknesses. The technique used in collecting these data is described in Chapter 3. A plot of this ratio is presented in Figure 19.
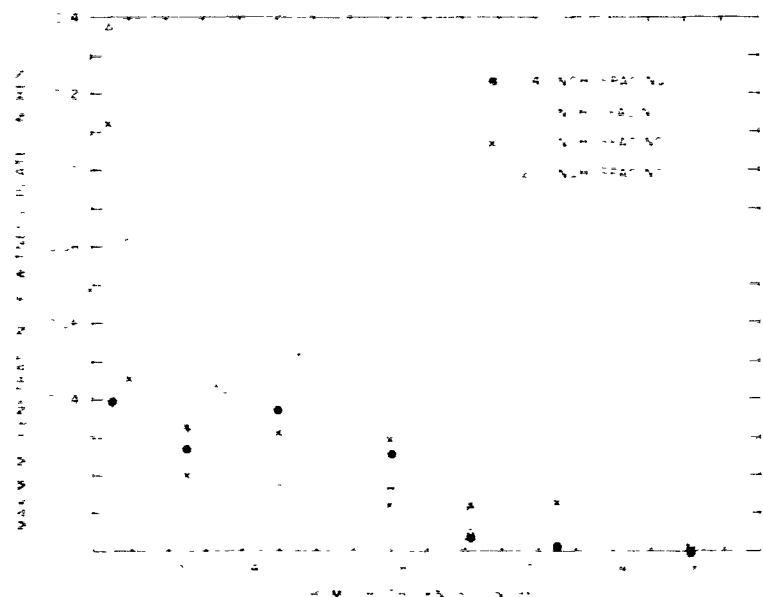

Figure 19. Plot of Momentum Ratio Across a Thin Bumper Target

DISCUSSION

As noted in the previous section, twenty-eight specially coated aluminum bumpers were successfully impacted and were returned to the Materials Laboratory at RTD for examination. Six targets were not included because they showed excessive particle

breakup. The conclusion reached by the Materials Laboratory as a result of its examination was that much of the emissive coating had been lost from the surface of these coated targets during the firing process. Further examination of the target submitted to RTD and of those remaining at our laboratory indicated that the removal of the coating was principally in the areas around impact of the accelerated particles.

It is speculated that this removal could have occurred either through effects caused by particulate matter striking the targets or from the effects of plasma associated with the firing of the hypervelocity gun. Since the initial temperature of the aluminum plasma is tens of thousands of degrees, it would seem possible that the aluminum oxide coating on the targets could have been melted or vaporized. Three facts, however, argue against this possibility. First, the plasma would be expected to affect the whole target almost uniformly at the 10 cm distances from gun to target. Second, in experiments designed to measure the momentum of accelerated particles, sheets of 0.001 in. thick aluminum foil were placed at these distances from the gun barrel; these foils were not vaporized as a result of firing. In this work there was evidence of heat distortion and many very small perforations produced by particulate debris several orders of magnitude smaller than the principal particle but, except for these effects, the thickness of the foil was substantially unchanged. Third, aluminum oxide has a very high melting point (2300°K) and heat of fusion (26 K-cal/mole) compared with aluminum itself (930°K and 2.6 K-cal/mole); thus, if even thin aluminum foil is not noticeably eroded by heat, one would hardly expect aluminum oxide films, deposited on good conductors, to be affected under the same conditions.

Closer examination of the target damage favors a different mechanism for coating removal during firing. On the target which we examined, a spray of particles produced a variety of impacts ranging from near penetrations to barely observable microcraters. Around each of these impacts, coating was removed to a diameter roughly four times that of the crater near the center of the damaged area (Figure 20). To ascertain whether a local high pressure impulse could cause this type of damage, an undamaged area of the target was dented with a spring loaded center punch. From Figure 21, it can be seen that the damage is very similar to that seen in Figure 20. In Figure 22, coating removal

Figure 20. 35X Enlargement of
Microcrater and Accompanying
Coating Removal

Figure 21. 35X Enlargement of Surface
Damage Done With Spring-Loaded
Center Punch

that took place on the rear surface of the target is also comparable. Since the rear of the target was not in direct contact with the incident plasma, it seems likely that the loss of coating is being caused by local high pressure impulsive loading and accompanying spaliation. It is, of course, possible that the incident plasma may aggravate such effects.
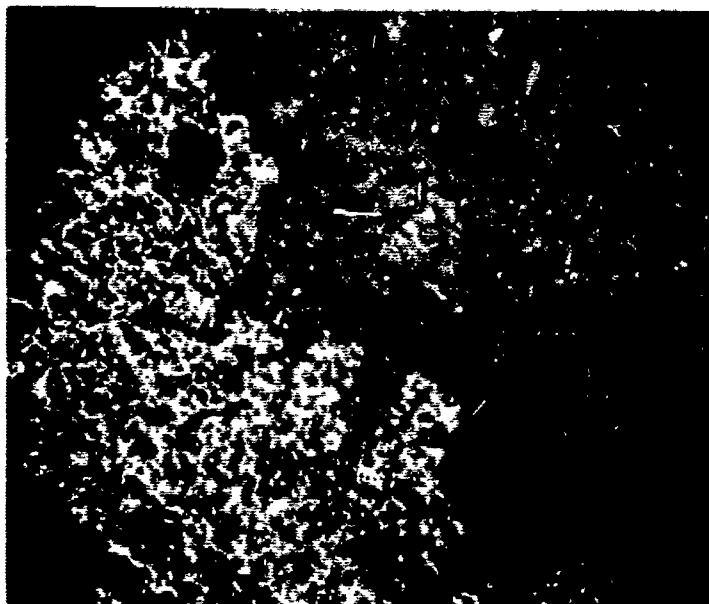

Figure 22. 35X Enlargement of Coating Removal on Back Surface

CONCLUSIONS

We conclude there is insufficient data presented for any one condition to justify a reasonable mathematical approximation of penetration resulting from target spacing, bumper thickness, or material properties. As improvements are made in the ability to control the parameters in the projection and analysis technique, the statistical value of each shot will be more meaningful. At this time, the results of this contract must be considered as an initial survey of data needed to solve a complex problem. However, under these circumstances, we can draw some preliminary conclusions.

1. Under all conditions encountered, the particle breaks up upon impacting the bumper. Usually, at least a hundred small craters were observed on the witness plate. This result was expected and is the primary reason bumpers are used for protection.

2. From our data, we observe very little dependence on bumper-to-target spacing, although this may be due to the inadequate data and to our tabulation of only the maximum penetration of the witness plate. Apparently the spacing is great enough so that the probability of two particles impacting the same crater is very small.

3. Even with the thinnest bumper and the closest spacing, the bumper offers substantial protection.

4. The reduction of momentum across the bumper appears to vary linearly with bumper

These results indicate that quantitative measurements are possible in this type of experiment. Further studies might profitably be directed toward measurement of momentum and energy per unit area on the witness plate.